Revision 2

Thermodynamic study of monoclinic pyrrhotite in equilibrium with pyrite in the Ag-Fe-S system by solid-state electrochemical cell technique

Dmitriy A. Chareev, Mikhail V. Voronin and Evgeniy G. Osadchii

Institute of Experimental Mineralogy, Russian Academy of Sciences, Chernogolovka, Moscow District, 142432, Russia. E-mail: chareev@iem.ac.ru

Abstract

An equilibrium mixture of monoclinic pyrrhotite and pyrite was synthesized in the eutectic $AlCl_3$-KCl melt at 525K. The reaction $7FeS_2(cr) + 12Ag(cr) = 8Fe_{0.875}S(cr) + 6Ag_2S(cr)$ was studied by an electromotive force technique in an all-solid-state electrochemical cell with an Ag^+ -conductive solid electrolyte in Ar at atmospheric pressure: (-) Pt | Ag | AgI | Ag_2S, $Fe_{0.875}S$, FeS_2 | Pt (+). In the 490K – 565K temperature range a linear electromotive force vs. temperature trend was obtained from which the temperature dependence of the sulfur fugacity was determined for the monoclinic pyrrhotite - pyrite equilibrium: $\log fS_2(mpo+py) = 14.079 - 14406 \cdot T^{-1}$, $(500<T/K<565)$. In addition, standard thermodynamic functions were calculated for monoclinic pyrrhotite $Fe_{0.875}S$ at 298K and atmospheric pressure: $\Delta G_f(mpo, 298.15K)$= -(136200 ±3000) $J \cdot mol^{-1}$, $S^o(mpo, 298.15K)$ = (66.7 ±1.3) $J \cdot mol^{-1} \cdot K^{-1}$, $\Delta H_f(mpo, 298.15K)$ = -(157400 ±3000) $J \cdot mol^{-1}$. Gaseous sulfur, S_2 – ideal gas at 1 bar (10^5 Pa) pressure was taken as a standard state for sulfur.

Keywords: monoclinic pyrrhotite, thermodynamic properties, sulfur fugacity, electrochemical cell technique, salt flux technique

Introduction

In most ore deposits one or several forms of iron sulfides are usually present, and they are often the prevailing ore components. The pyrrhotite (po) – pyrite (py) equilibrium and pyrrhotite as a phase of variable composition are often used as a sulfur fugacity indicator (Toulmin and Barton, 1964; Barton and Toulmin, 1966; Scott, 1976).

There are three stable sulfides in the Fe-S system in the 500-750K temperature interval: stoichiometric pyrite FeS_2, anti-ferromagnetic hexagonal β-pyrrhotite (β-po), which is stable below 598K, and paramagnetic hexagonal γ-pyrrhotite (γ-po), stable at temperatures above 598K (Toulmin and Barton, 1964), or 601K (Osadchii and Chareev, 2006). The transition of pyrrhotite from the β-phase into the γ-phase occurs at 598 ±8K and is accompanied by a change of the magnetic properties.

Low temperature phase relations in the Fe-S system were studied in several works. According to Nakazawa and Morimoto (1971) in the region of β-po stability at least nine pyrrhotite superstructures were isolated, but no data on their stability were reported. The most well known naturally-occurring superstructure is $Fe_{0.875}S$ (Fe_7S_8), monoclinic pyrrhotite (mpo), occurring in equilibrium with pyrite. Taylor (1970) concluded that the peritectoid transformation mpo↔po+py, occurring at 565K, is metastable, whereas according to Kissin and Scott (1982), this transition is stable and occurs at 527K.

In nature, monoclinic pyrrhotite is found in equilibrium with pyrite or pyrrhotite superstructures of various compositions including troilite. This observation suggests instability of all pyrrhotite superstructures except for monoclinic pyrrhotite and troilite (Putnis and McConnell, 1980).

In our previous study (Osadchii and Chareev, 2006) in the temperature range of 518-723K only hexagonal pyrrhotite was stable in an assemblage with pyrite and argentite. On cooling of the Ag-Fe-S system below 518 K a phase reaction β-po + arg → Ag + py occurs,

silver appears in the sample system, and the electromotive force (EMF) of the cell becomes zero (E=0). At the same time the growth of threadlike silver crystals on the free surface of the sample was observed. Further, increasing the temperature above 518K, leads to a new linear $E(T)$ trend that is different from the previously obtained *E(T)* dependence for the β-po+py equilibrium (Chareev and Osadchii, 2005). Such trends had a smaller slope in *E-T* coordinates and always intersected with the β-po+py equilibrium line below the β-γ transition point in hexagonal pyrrhotite (~574K). The position of these trends depended on the given annealing temperature (below 518 K) and the exposure time and was related to the formation of metastable monoclinic pyrrhotite, differing from the equilibrium β-po by the higher sulfur content. However no evidence of the presence of exactly monoclinic pyrrhotite in the sample system was found.

Theoretical background

Equilibrium phase relations in the Ag-Fe-S system that include monoclinic pyrrhotite, pyrite and argentite are described by the solid state reaction

$$7FeS_2(cr) + 12Ag(cr) = 8Fe_{0.875}S(cr) + 6Ag_2S(cr) \quad (1).$$

Reaction (1) can be implemented in an all-solid-state electrochemical cell

(-) Pt | Ag | AgI | Ag_2S, $Fe_{0.875}S$, FeS_2 | Pt (+)

The cell can be represented as two half-cells:

Left half-cell (reference system):

$$12Ag(cr) = 12Ag^+ + 12e$$

Right half-cell (sample system):

$$12Ag^+ + 12e + 7FeS_2(cr) = 6Ag_2S(cr) + 8Fe_{0.875}S(cr)$$

and the overall potential forming process coincides with reaction (1).

The equilibrium EMF (E) of the electrochemical cell involving silver sulfide can vary from zero when the sample system (on the right) contains metallic silver and sulfur fugacity (fS_2) corresponds to Ag-Ag_2S equilibrium, to its maximum value when the sample system contains liquid sulfur.

EMF of the cell is related to the reaction free energy by the equation

$$\Delta G_r = -nFE \quad (2),$$

where ΔG_r ($J \cdot mol^{-1}$) is the free energy change in the course of the reaction; n=12 is the number of electrons participating in the electrochemical process; F = 96485.309 $C \cdot mol^{-1}$ is the Faraday constant; E is the EMF of the electrochemical cell in volts.

Therefore, knowing ΔG_r of the reaction (1), the Gibbs energy of silver sulfide and pyrite, it is possible to find the temperature dependence of the Gibbs energy of monoclinic pyrrhotite:

$$\Delta G_f(Fe_{0.875}S, cr) = -3/2FE + 7/8\Delta G_f(FeS_2, cr) - 3/4\Delta G_f(Ag_2S, cr) \quad (3)$$

Using $\Delta G_f(Fe_{0.875}S, cr)$, calculated from the equation (3), and $\Delta G_f(FeS_2, cr)$, taken from the literature, one can calculate the sulfur fugacity for the mpo-py equilibrium

$$Fe_{0.875}S + 3/8S_2 = 7/8FeS_2 \quad (4)$$

according to:

$$\log fS_2 = [7/8\Delta G_f(FeS_2, cr) - \Delta G_f(Fe_{0.875}S, cr)]/(3/8RT\ln 10) \quad (5)$$

where R is the gas constant, (8.314510 $J \cdot K^{-1} \cdot mol^{-1}$); T is the absolute temperature; and gaseous sulfur ($S_{2,gas}$) is taken as the reference state for sulfur.

Substituting $\Delta G_f(Fe_{0.875}S, cr)$ from the equation (3) into equation (5) we get:

$$\log fS_2(mpo/py) = [\Delta G_f(Ag_2S, cr) + 2FE]/0.5RT\ln 10 \quad (6).$$

Thus, the sulfur fugacity for the mpo/py equilibrium can be obtained directly from measuring EMF of the cell (A) using thermodynamic data for Ag_2S only.

Using additional data for temperature dependence of the free energy of formation of argentite from silver and S_2(g) from Richardson and Jeffes (1952)

$$\Delta G_f(Ag_2S, cr) = -87822 + 34.56 \cdot T, \quad J \cdot mol^{-1} \qquad (7),$$

we obtain the equation

$$\log fS_2 = (-9174.5 + 20.159 \cdot E/mV) \cdot T^{-1} + 3.61 \qquad (8),$$

which in this temperature interval practically coincides with the newer data from Barin (1995), Robie and Hemingway (1995), and applicable for studying any sulfide solid state equilibria involving Ag_2S.

Experimental

The assemblage monoclinic pyrrhotite — pyrite was synthesized in silica-glass ampoules containing an eutectic KCl-$AlCl_3$ melt (~66 atomic % $AlCl_3$) with a melting temperature below 427 K (Moh and Taylor, 1971). Previously we used this eutectic mixture for synthesis of $FeSe_{1-\delta}$ crystals at ~673K (Chareev et al, 2013). The synthesis temperature and a batch composition were chosen according to the Fe-S phase diagram of Nakazawa and Morimoto (1971).

Reagents used were carbonyl iron (Merck, 99.5%, 10 μm), crystalline sulfur (Johnson Matthey, 99.9995%), KCl and anhydrous $AlCl_3$ (Fluka, 98%). The volume of salts was approximately four times greater than that of sulfides. Silica-glass ampoules were heated to 523K – 528K, left for up to three months and were shaken occasionally to mix the batch. The resulting iron sulfides were washed from the salt eutectic in distilled water, alcohol and acetone in ultrasound bath.

The chemical composition of iron sulfides was studied with a digital scanning electronic microscope TESCAN Vega II XMU with the energy dispersive micro analysis system INCA Energy 450/XT (20 kV). The analysis showed that the approximate chemical

124 composition of the phases was close to $Fe_{0.875}S$ and FeS_2. No impurity elements (K, Al, Cl)
125 were found.

126 The obtained samples were studied using the X-ray powder diffractometry (DRON-7,
127 CoK_α radiation, Fe filter), Fig. 1, and were compared with JCPDS data. The composition of
128 the monoclinic pyrrhotite in the synthesized mpo+py assemblage was evaluated using the
129 method suggested by Yund and Hall (1969). For this purpose the initial mpo+py mixture in an
130 evacuated ampoule was placed into the furnace at 650K and left for 30 minutes and then was
131 quenched in cold water. During the heating vacancy disordering occurs in the iron sublattice
132 and monoclinic pyrrhotite transforms into hexagonal pyrrhotite. The composition of the
133 obtained hexagonal pyrrhotite (Fig1, inset) was determined from the (102) reflection using the
134 X-ray analytical dependence from Yund and Hall (1969). The DRON-7 diffractometer, the
135 CoK_α radiation, the Fe filter, a scanning step $\theta = 0.01^o$, and the external standard — silica,
136 were also used for that purpose.

137 The working electrode was prepared from the mixture of the synthesized iron sulfides
138 and Ag_2S (Aldrich Chem. Co., 99.9%) of the 1:1 mass ratio and the total weight of 400 mg,
139 which was pressed into a tablet of 6 mm diameter under the loading of 1-1.2 tons. The
140 reference electrode of metallic silver and the AgI solid electrolyte were also pressed into
141 tablets of 6 mm diameter and approximately of 3 mm thickness. The inert platinum electrodes
142 of 6 mm diameter were cut out from a sheet of 0.5 mm thickness.

143 The temperature dependence of EMF was obtained by the "temperature titration"
144 technique, i.e. waiting till the value of EMF becomes constant (equilibrium) at the given
145 temperature. The equilibrium was considered achieved when the value of EMF stayed
146 constant within the limits of ±0.03 mV for several days. The EMF of the cell (A) was
147 measured in the temperature interval of 498K – 731K (Appendix). It took a rather long time
148 (up to 2-3 weeks) to achieve equilibrium EMF values in contrast to similar cells with

hexagonal pyrrhotite (Osadchii and Chareev, 2006), that were studied in the same temperature interval.

There were no attempts to study EMF of the cell at temperatures definitely lower than the temperature of stability of the po-py-Ag_2S association ($T \leq 500$K, $E=0$), as described in the work of Chareev and Osadchii (2005), since there was always a possibility of an irreversible decomposition or a composition change in the monoclinic pyrrhotite. The design of the cell and the measurement technique were examined in detail in the works of Osadchii and Chareev (2006) and Osadchii and Echmaeva (2007).

Results and discussion

Fig. 1 (inset) shows in coordinates relative intensity – 2θ the shape of the ($40\,\overline{8}$, $22\,\overline{8}$, 228, 408) quadruplet of the synthesized monoclinic pyrrhotite and the shape of the (102) peak of the hexagonal pyrrhotite, obtained by annealing of this monoclinic pyrrhotite. Also the figure shows the theoretical positions of monoclinic pyrrhotite peaks according to MINCRYST X-ray database (Chichagov et al, 1990). The synthesized monoclinic pyrrhotite has the 2θ position which is less than that of monoclinic pyrrhotite according to Chichagov et al. (1990), and should be richer in iron. In contrast, synthetic pyrrhotite transformed into a hexagonal form, has the 2θ position which is larger than that of hexagonal $Fe_{0.875}S$ pyrrhotite and corresponds to the composition $Fe_{0.865\pm0.004}S$. Taking into account this contradiction, practically stoichiometric compositions of natural monoclinic pyrrhotites, and an implausible bend of the mpo-py solvus from Kissin and Scott (1982), it was assumed for subsequent calculations that the synthesized pyrrhotite also has the $Fe_{0.875}S$ composition (the Fe_7S_8 stoichiometry).

The high-temperature (above 565K) nonlinear part of the $E(T)$ trend likely corresponds to non-equilibrium decomposition of monoclinic pyrrhotite. The low temperature

part (22 points, Appendix), corresponds to the monoclinic pyrrhotite – pyrite equilibrium and is approximated by the linear equation ($\Delta_r C_p = 0$):

$$E(\text{mpo+py}), \text{mV} = -(260.1 \pm 4.1) + (0.5205 \pm 0.0080)\cdot T, \ (498<T/\text{K}<560) \ R^2=0.9999 \qquad (9)$$

Experimental errors were determined by the least square method for the confidence interval of 2σ.

Substituting Eq. (9) into Eq. (8) we obtain the equation of the temperature dependence of the sulfur fugacity along the equilibrium monoclinic pyrrhotite - pyrite:

$$\log fS_2(\text{mpo+py}) = 14.079 - 14406\cdot T^{-1} \qquad (10)$$

Then from equation (5), using the Gibbs free energy vs temperature data of Toulmin and Barton (1964):

$$\Delta G_f(FeS_2, \text{cr}) = -298236 + 196.98\cdot T, \ (\text{J}\cdot\text{mol}^{-1}) \qquad (11)$$

and equation (10) for the sulfur fugacity, we obtain the temperature dependence of the Gibbs energy of formation of monoclinic pyrrhotite from α-Fe and gaseous sulfur S_2:

$$\Delta G_f(Fe_{0.875}S, \text{mpo}) = -157400 + 71.11\cdot T \qquad (12)$$

The calculation of the sulfur fugacity for the mpo+py equilibrium definitely has a greater accuracy than $\Delta_f G_{T(\text{mpo})}$, since the absolute value and the accuracy of fS_2 mostly depend on the choice and the accuracy of thermodynamic data for Ag_2S, and switching to thermodynamic properties of mpo requires the knowledge of the thermodynamic properties of pyrite and monoclinic pyrrhotite and the composition of monoclinic pyrrhotite. Therefore, the calculation of the thermodynamic properties of monoclinic pyrrhotite is given for comparison only. It should be noted that the change in the composition of pyrrhotite from $Fe_{0.875}S$ to $Fe_{0.865}S$ changes ΔG_f(mpo, 298.15K) for only 400 $\text{J}\cdot\text{mol}^{-1}$ which is much less than the measurement errors (3000 $\text{J}\cdot\text{mol}^{-1}$).

Thermodynamic data obtained for monoclinic pyrrhotite as well as additional data used are shown in Table 1. Fig 2 shows major equilibria discussed in this work in the logfS_2 – reciprocal temperature coordinates.

The analysis of Table 1 shows that the enthalpy of formation of mpo practically matches the literature data (Robie and Hemingway, 1995; Xu and Navrotsky, 2010), while the entropy on the contrary is noticeably higher. The curve of the sulfur fugacity calculated from the literature data (Fig. 2), is at a small angle to the β-po+py dependence, and the extrapolation to the intersection with the γ-po+py curve leads to confirmation of stability of monoclinic pyrrhotite up to the highest temperatures. The mpo-py equilibrium we measured (Fig. 2, solid circles) lies noticeably lower than predictions of literature thermodynamic data (dashed and dotted lines) and has a slightly different temperature slope. Our data are also located at a larger angle to the β-po+py equilibrium compared with the Robie and Hemingway (1995) data. What is most important, at temperatures above ~565K one can see a slight deviation from the low temperature linear trend for the mpo+py equilibrium (Fig. 2, open circles). This behavior can be explained by a slow sulfur loss of monoclinic pyrrhotite due to the peritectoid decomposition reaction of monoclinic pyrrhotite $Fe_7S_8 \rightarrow$ β-$Fe_{1-x}S$ + FeS_2, occurring in the temperature interval of 550K – 600K. We expect that in the absence of kinetic constraints the decomposition of mpo into β-po+py would occur at lower temperatures, as indicated by an arrow in Fig. 2.

Implications

A rather small difference in the sulfur fugacity for the mpo – py equilibrium as compared to that of the hexagonal β-po – py equilibrium confirms the possibility of coexistence of various structures of pyrrhotite under the similar physicochemical conditions, which is often observed in natural objects.

The authors thank T.N. Dokina for performing X-ray studies, K.V. Van for performing the microprobe analysis, N.V. Lichkova for the synthesis of AgI, and A.V. Plyasunov for useful discussions. The constructive and helpful review comments of S.A. Kissin are gratefully acknowledged.

References

Barin, I. (1995) Thermochemical Data of Pure Substances, 3rd ed., 2 vols., VCH Publishing: Weinheim.

Barton, P.B., and Toulmin, P. (1966) Phase relations involving sphalerite in the Fe-Zn-S system. Economic Geology 61, 815-849.

Chareev, D.A., and Osadchii, E.G. (2005) Pyrrhotite-pyrite equilibria in the Ag-Fe-S system at 245 to 310°C and standard pressure. Geochemistry, Mineralogy and Petrology, Bulgarian Academy of Sciences, 43, 41-46.

Chareev, D., Osadchii, E., Kuzmicheva, T., Lin, J.-Y., Kuzmichev, S., Volkova, O.S., and Vasiliev, A.N. (2013) Single crystal growth and characterization of tetragonal $FeSe_{1-x}$ superconductors, CrystEngComm, 2013,15, 1989-1993.

Chichagov, A.V., Belonozhko, A.B., Lopatin, A.L., Dokina, T.N., Samokhvalova, O.L., Ushakovskaya, T.V., and Shilova, Z.V. (1990) Information-calculating system on crystal

structure data for minerals (MINCRYST). Kristallografiya, 35. 3, 610-616 (in Russian). http://database.iem.ac.ru/mincryst/

Kissin, S.A., and Scott, S.D. (1982) Phase relations involving pyrrhotite below 350°C. Economic Geology 77, 1739-1754.

Moh, G.H., and Taylor, L.A. (1971) Laboratory techniques in experimental sulfide petrology. Neues Jahrbuch für Mineralogie – Monatshefte, 10, 450 – 459.

Nakazawa, H., and Morimoto, N. (1971) Phase relations and superstructures of pyrrhotite, $Fe_{1-x}S$. Materials Research Bulletin, 6, 345-358.

Osadchii, E.G., and Chareev, D.A. (2006) Thermodynamic studies of pyrrhotite-pyrite equilibria in the Ag-Fe-S system by solid-state electrochemical cell technique at 518 to 723 K and total pressure of 1 atm. Geochimica et Cosmochimica Acta, 70, 5617-5633.

Osadchii, E.G., and Echmaeva, E.A. (2007) The system Ag-Au-Se: Phase relations below 405 K and determination of standard thermodynamic properties of selenides by solid-state electrochemical cell technique. American Mineralogist, 92, 640–647.

Putnis A., McConnell J. D. C. (1980) Principles of mineral behaviour. Elsevier.

Richardson, F.D., and Jeffes, J.H.E. (1952) The thermodynamics of substances of interest in iron and steel making. Journal of the iron and steel institute 165-175.

Robie, R.A., and Hemingway, B.S. (1995) Thermodynamic properties of minerals and related substances at 298.15 K and 1 Bar (10^5 Pascals) pressure and at high temperatures. U.S. Geological Survey Bulletin 2131.

Scott, S.D. (1976) Application of the sphalerite geobarometer to regionally metamorphosed terrains. American Mineralogist 61, 661-670.

Taylor, L.A. (1970) The system Ag-Fe-S: phase equilibria and mineral assamblages. Mineralum Deposita 5, 41-58.

Toulmin P., III, and Barton, P.B. Jr. (1964) A thermodynamic study of pyrite and pyrrhotite. Geochimica et Cosmochimica Acta 28, 641-671.

Xu, F., and Navrotsky, A. (2010). Enthalpies of formation of pyrrhotite $Fe_{1-0.125\ x}S$ ($0 \leq x \leq 1$) solid solutions. American Mineralogist, 95, 717-723.

Yund, R.A., and Hall, H.T. (1969) Hexagonal and monoclinic pyrrhotites. Economic Geology 64, 420-423.

292 **Table 1.** Thermodynamic properties of monoclinic pyrrhotite at 298.15 K and 1 bar pressure

293 and auxiliary data. The standard state for sulfur - ideal S_2 gas at p = 1 bar

Phase	$\Delta_f G^o$	$\Delta_f H^o$	S^o	References
	$J \cdot mol^{-1}$	$J \cdot mol^{-1}$	$J \cdot mol^{-1} \cdot K^{-1}$	
Fe(cr)	0	0	27.09 ±0.13	(Robie, Hemingway, 1995)
S_2(g)	0	0	228.17 ±0.02	(Robie, Hemingway, 1995)
S(cr)	-39726 ±335	-64245 ±250	15.511 ±0.05	(Robie, Hemingway, 1995)
FeS_2 (pyrite)	-239800 ±1700	-300100 ±1700	52.9 ±0.1	(Robie, Hemingway, 1995)
FeS_2 (pyrite)	-239500 ±2100	-298240 ±2100	58.3 ±0.2	(Toulmin, Barton, 1964)
$Fe_{0.875}S$(mpo)	-138800 ±2000	-161800 ±2000	60.79 ± 0.21	(Robie, Hemingway, 1995)
$Fe_{0.875}S$(β-po))		-158650 ±3000		(Xu, Navrotsky, 2010)
$Fe_{0.875}S$ (mpo)*	-140100 ±3000	-166500 ±3000	49.2 ± 0.3	(Chareev, Osadchii, 2005)
$Fe_{0.875}S$(mpo)	-136200 ±3000	-157400 ±3000	66.7 ± 1.3	present study

294 * the mpo composition and structure has not been proved

295

296

297 **Figure captions**

298

299 **Fig. 1.** X-ray diagram of the monoclinic pyrrhotite (mpo) – pyrite (py) assembage. In the
300 inset: monoclinic pyrrhotite ($40\,\overline{8}$, $22\,\overline{8}$, 228, 408) quadruplet (this study and Chichagov et al,
301 1990) and (102) peak of hexagonal pyrrhotite (β-po) formed after annealing of monoclinic
302 pyrrhotite.

303

304 **Fig. 2.** Sulfur fugacity vs reciprocal temperature in the Ag-Fe-S system. Solid circles are the
305 sulfur fugacity measured for the monoclinic pyrrhotite - pyrite equilibrium. Open circles are
306 experimental points not included in calculation due to the mpo decomposition (See
307 Appendix). Also the plot shows fugacity dependences for β-po+py and γ-po+py equilibria
308 (Osadchii, Chareev, 2006); Ag_2S(arg)+Ag (Richardson, Jeffes, 1952), and the monoclinic
309 pyrrhotite -pyrite equilibrium calculated using data from (Robie, Hemingway, 1995) for mpo
310 and data from (Toulmin, Barton, 1964) for py, and calculated using data from (Robie,
311 Hemingway, 1995) for both pyrite and monoclinic pyrrhotite; the sulfur condensation curve
312 S(l)/S_2(gas) using data from Barin (1995) (the upper left corner).

313

314

315

APPENDIX

Measured temperatures and EMF (mV) of the electrochemical cell and deviations between the experimental points and Eqn. (9)

T (K)	E_{meas} (mV)	E_{meas} - E_{calc}
498.4*	0.71	1.43
500.3	0.12	-0.15
500.5	0.47	0.1
501.3	0.78	-0.01
501.6	0.96	0.05
504.2	2.55	0.26
504.3	2.21	-0.11
505.4	2.95	0.04
506.1	2.92	-0.37
509.7	5.02	-0.12
510.2	5.48	0.06
511.4	5.6	-0.42
513.3	6.91	-0.09
515.9	8.45	0.05
516.1	8.28	-0.2
517.7	9.19	-0.14
517.9	10.16	0.72
519.8	10.55	0.14
522.6	12.05	0.21
523.7	12.7	0.26
531.3	16.4	-0.01

541.6	21.71	-0.05
551.7	26.75	-0.23
561.6*	31.66	-0.52
572.0*	36.37	-1.22
587.2*	43.8	-1.66
597.4*	49.43	-1.36
607.9*	55.14	-1.1
617.9*	60.92	-0.53
628.2*	66.44	-0.4
638.6*	72.23	-0.01
648.7*	77.65	0.17
658.9*	83.80	0.98
669.4*	89.98	1.72
679.6*	95.81	2.26
690.3*	101.59	2.43
696.1*	104.90	2.76
700.7*	107.85	3.29
706.1*	110.74	3.36
710.8*	113.76	3.92
716.2*	116.67	4.04
721.0*	119.84	4.74
731.1*	125.8	5.44

319 (*) points are excluded from calculations but shown in Fig. 2.

320

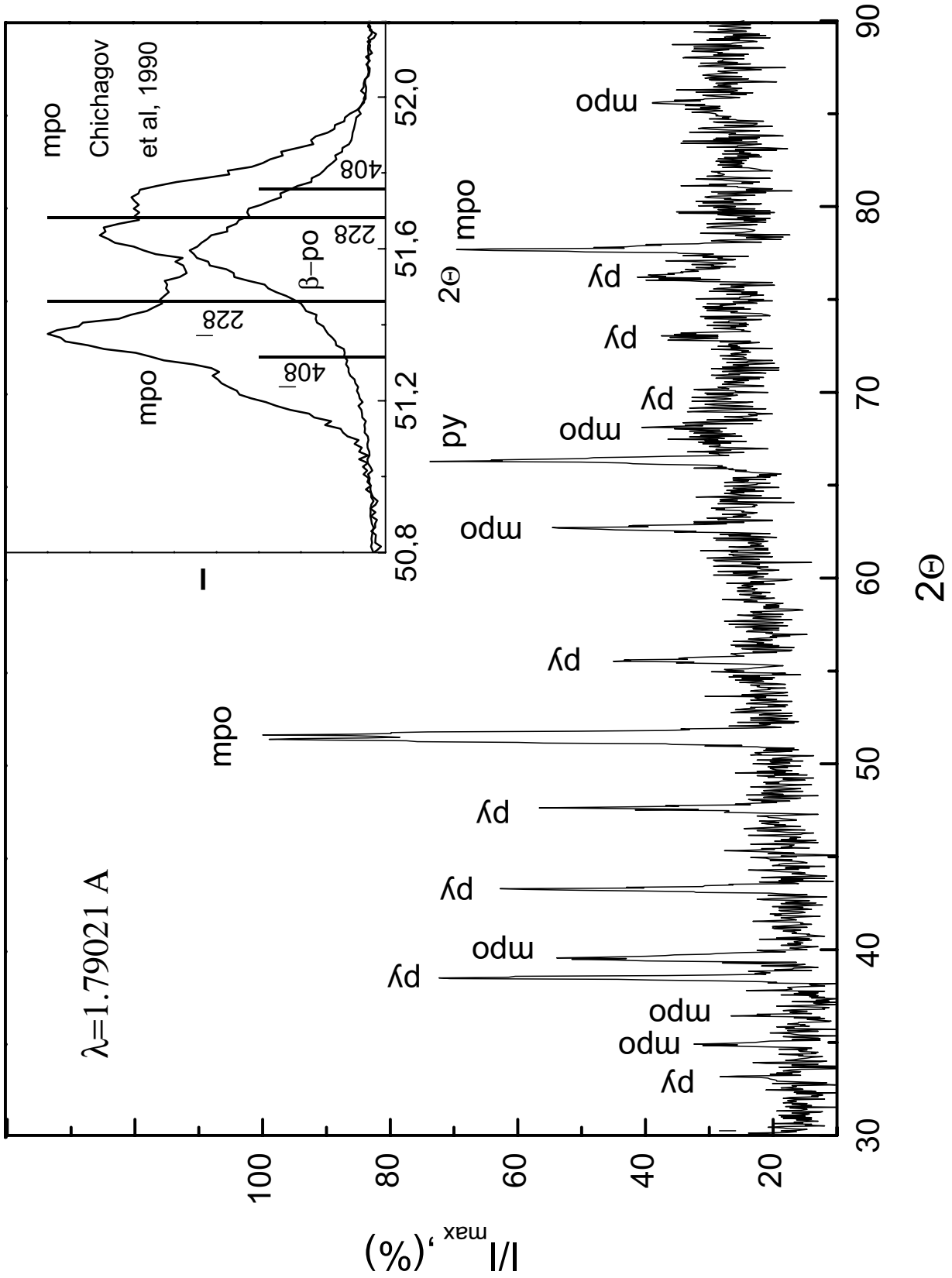
λ=1.79021 A
I/I max,(%)
2Θ
mpo
py
ad
β–po
Chichagov
et al, 1990
228
408

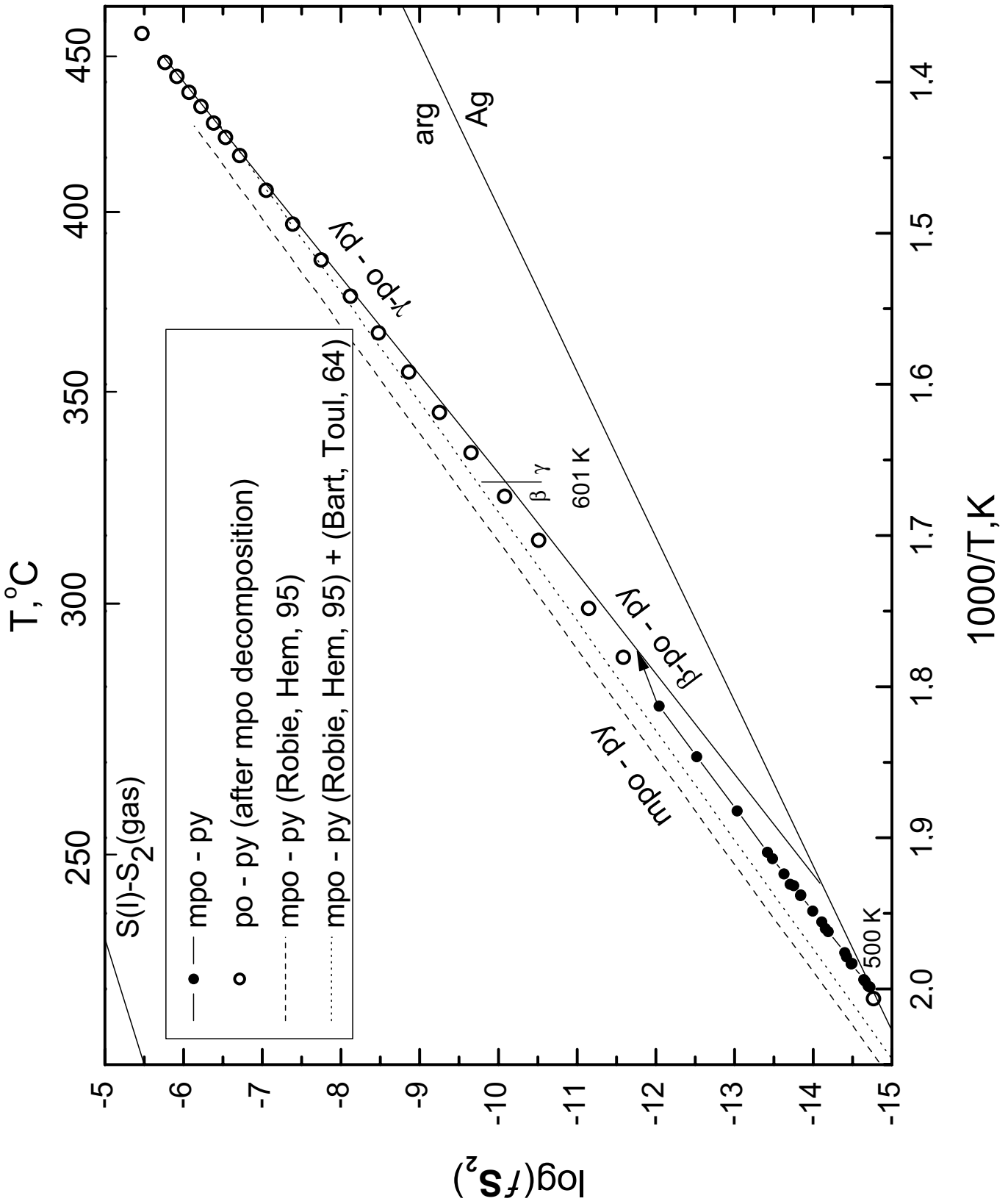
T,°C
1000/T,K
log(fS2)
S(l)-S2(gas)
mpo - py
po - py (after mpo decomposition)
mpo - py (Robie, Hem, 95)
mpo - py (Robie, Hem, 95) + (Bart, Toul, 64)
arg
Ag
γ-po - py
β-po - py
mpo - py
601 K
500 K
β
γ